Research Article

Statistical Optimization of Operational Parameters for Enhanced Naphthalene Degradation by TiO_2/Fe_3O_4-SiO_2 Photocatalyst

Aijuan Zhou,[1] Jing Peng,[2] Zhaobo Chen,[3,4] Jingwen Du,[1] Zechong Guo,[1] Nanqi Ren,[1,3] and Aijie Wang[1,3]

[1] *School of Municipal and Environmental Engineering, Harbin Institute of Technology (HIT), 202 Haihe Road, Harbin 150090, China*
[2] *Institute of Architecture Design and Research, Harbin Institute of Technology, Harbin 150090, China*
[3] *State Key Laboratory of Urban Water Resource and Environment, Harbin Institute of Technology (SKLUWRE, HIT), Harbin 150090, China*
[4] *Collage of Materials Science and Chemical Engineering, Harbin Engineering University, Harbin 150001, China*

Correspondence should be addressed to Aijie Wang, waj0578@hit.edu.cn

The optimization of operational parameters for enhanced naphthalene degradation by TiO_2/Fe_3O_4-SiO_2 (TFS) photocatalyst was conducted using statistical experimental design and analysis. Central composite design method of response surface methodology (RSM) was adopted to investigate the optimum value of the selected factors for achieving maximum naphthalene degradation. Experimental results showed that irradiation time, pH, and TFS photocatalyst loading had significant influence on naphthalene degradation and the maximum degradation rate of 97.39% was predicted when the operational parameters were irradiation time 97.1 min, pH 2.1, and catalyst loading 0.962 g/L, respectively. The results were further verified by repeated experiments under optimal conditions. The excellent correlation between predicted and measured values further confirmed the validity and practicability of this statistical optimum strategy.

1. Introduction

Naphthalene, as the first member of polycyclic aromatic hydrocarbon (PAH) and one of the 16 PAHs classified as priority pollutants by the Environmental Protection Agency (EPA) of the United States, is a class of persistent organic pollutants of special concern. Naphthalene can be frequently found in many anthropogenic fluxes, such as combustion fumes, used oil, and bilge water, which is exceedingly recalcitrant to degradation due to its inhibitory nature [1–3]. Since it is the most water-soluble PAH, naphthalene is the dominant one in water which has been considered as possibly a carcinogen to humans (EPA 1998, The International Agency for Research on Cancer (IARC) 2002) and has both acute and chronic effects on human and animal health.

A solution to this naphthalene pollution problem has now become urgent. Removing naphthalene from water is possible via many techniques, including biofiltration [4], microbial degradation [5, 6], anaerobic degradation [7–9], electron beam irradiation [10], electrolytic aeration [11], and photocatalysis [12–14]. Among these techniques, biodegradation is expected to be an economical and energy-efficient approach which attracts more and more attentions to investigate the application to treat PAHs. Nevertheless, because of its toxicity and low water solubility, the efficacy of bioremediation still remains a critical point [15].

Photocatalysis has been proposed as an alternative to degrade refractory organic compounds unquestionably due to the specificity of hydroxyl radicals which represents high reaction rate and low selectivity [16–19]. Although this technique presents critical advantages over other techniques, there are some problems to be resolved urgently. Among these, the commonly mentioned problems are the designs of adequate reactors for efficient utilization of photons and the required higher degradability to persistent organic pollutants. Moreover, this technology has not been successfully commercialized, in part because of the difficulty in separating TiO_2 nanoparticles from the suspension [20]. To resolve

this problem, TiO$_2$ dispersed on magnetic oxide support (Fe$_3$O$_4$-SiO$_2$) is used in this study as the catalyst for photooxidative degradation of naphthalene which could be reclaimed using ferromagnetic separation processes.

In order to enhance the naphthalene degradation performance, an optimization approach should be employed. Response surface methodology (RSM) is an efficient standard and well-established mathematical optimization procedure which can achieve such an optimization by analyzing and modeling the effects of multiple variables and their responses and finally optimizing the process [21]. This method has been successfully employed for optimization in some photocatalytic oxidation processes [22–26]. However, to the best of our knowledge, the optimization of photocatalytic degradation of naphthalene solution by TiO$_2$/Fe$_3$O$_4$-SiO$_2$(TFS) catalyst has not been reported. Therefore, the objective of this study was to investigate the effect of TiO$_2$/Fe$_3$O$_4$-SiO$_2$(TFS) photocatalyst on the treatment of a simulated high-concentration wastewater polluted by naphthalene. The central composite circumscribed (CCC) design method of RSM was employed to determine the optimal process condition for maximizing naphthalene degradation rate.

2. Materials and Methods

2.1. Reagents and Photocatalyst Preparation. FeCl$_2$, FeCl$_3$, NaOH, HNO$_3$, Fe$_3$O$_4$, absolute alcohol, and isopropanol (Tianjin Kermel Chemical Reagent Co. Ltd.) were of analytical grade; naphthalene (Aldrich), Ti(OC$_4$H$_9$)$_4$, 3-aminopropyltriethoxysilane, and tetraethoxysilane (J&K Chemical Ltd Co.) were of reagent grad; all the reagents mentioned above were used as received without further purification. Millipore deionized water was used for dilution.

For now, the TFS photocatalyst has been prepared successfully, and the specific preparation and characterization have been published in other paper [27]. The synthesis route of TFS photocatalyst is shown in Figure 1.

2.2. Photoreactor. A schematic representation of the photoreactor is shown in Figure 2. The reactor mainly consisted of mechanical stirrer, mercury lamp, quartz cold trap, and beaker. The irradiation experiments were carried out in four parallel 250 mL quartz beakers. The light source was a high-pressure mercury lamp (HPK 125W, Philips) setting in a quartzose cold trap, emitting the near-UV (mainly around 365 nm). The warp of photoreactor was made of polymethyl methacrylate (PMMA), inner surface of which clings silver paper in order to return UV light.

2.3. Multivariate Experimental Design. A 3-factor CCC with six replicates at the center point leading to 20 experiments was employed to optimize the operational parameters for improving naphthalene degradation. For statistical calculation, the relation between the coded values and actual values of independent variable is described as follows.

$$X_i = \frac{A_i - A_0}{\Delta A_i}, \tag{1}$$

where X_i is the coded value of the independent variable, A_i is the actual value of independent variable, A_0 is the actual value of the A_i at the center point, and ΔA_i is the step change of independent variable.

In the study, catalyst loading, pH, and irradiation time were taken as the independent variable and naphthalene degradation rate was the dependent variable or response of the design experiments. By means of multilinear regression method [28, 29], a second-order polynomial function was fitted to correlate relationship between independent variable and response. Quadratic equation for the independent variable was expressed as follows.

$$\begin{aligned} y = {} & \beta_0 + \beta_1 x_1 + \beta_2 x_2 + \beta_3 x_3 + \beta_{11} x_1{}^2 \\ & + \beta_{22} x_2{}^2 + \beta_{33} x_3{}^2 + \beta_{12} x_1 x_2 + \beta_{13} x_1 x_3 + \beta_{23} x_2 x_3, \end{aligned} \tag{2}$$

where y represents the predicted response; β_0 is the interception coefficient; β_1, β_2, and β_3 are the linear coefficients; β_{11}, β_{22}, and β_{33} are the quadratic coefficients; β_{12}, β_{13}, and β_{23} are the interactive coefficients; x_1, x_2, and x_3 represent the independent variable studied.

The Design Expert (Version 7.4.1.0, Stat-Ease Inc., Minneapolis, MN, USA) software was used for regression and graphical analyzes of the data obtained. All experimental designs were randomized, and mean values were applied.

2.4. Procedure. As the solubility of naphthalene is 25–30 mg/L at ambient temperature, this study chose to work with the highest concentration in order to show the unique removal efficiency of TFS photocatalyst [3]. In all the photocatalytic experiments, the reaction temperature was kept constant at $25 \pm 0.1°$C. Unless required, pH was not initially modified or controlled in the reactor. When required, initial pH values were adjusted using 4 mol/L NaOH or H$_2$SO$_4$.

All experiments were carried out in 250 mL quartzose beakers comprised of 100 mL aqueous naphthalene solution and the appropriate amount of the TFS photocatalyst powder, stirring at 1000 rpm (higher rotated speed may result in naphthalene volatilization without degradation). Before irradiation, the reaction mixture was premixed in the dark for 20 min to reach adsorption equilibrium.

2.5. Analytical Methods. The residual naphthalene was determined by a high-performance liquid chromatography (LC-10A, Shimadzu Corporation, Kyoto, Japan) equipped with a diode array detector and an Uptisphere C18 HDO column (stationary phase 3 μm, dimensions 150 mm $\times$ 3 mm) using a mixture of methanol and deionized water (ratio 80 : 20) as the mobile phase at a flow rate of 1.0 mL/min.

3. Results and Discussion

3.1. Effect of Catalyst Loading on Degradation of Naphthalene. The catalyst loading in slurry photocatalytic processes was an important factor. Figure 3 presents the variation of the first order rate constant and the value of Ct/Co as a function of the catalyst loading, where Ct is the naphthalene concentration at t time and Co is the initial concentration of naphthalene.
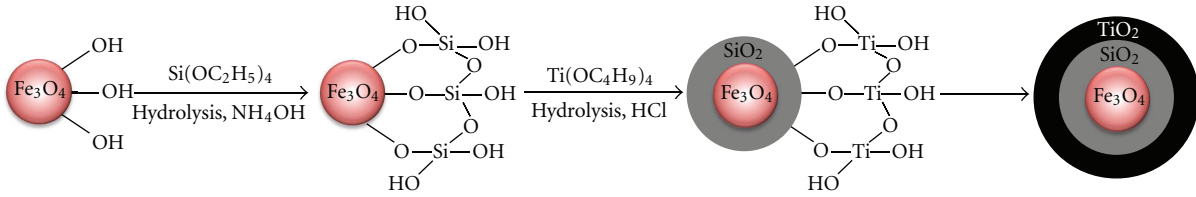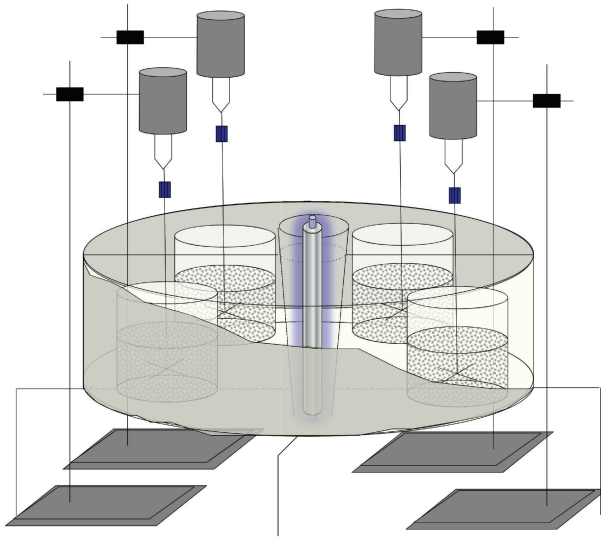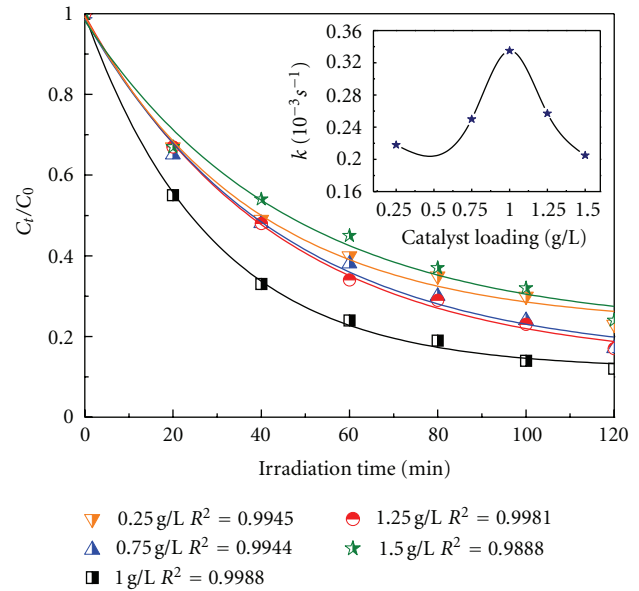
FIGURE 1: Synthesis route of TiO_2/Fe_3O_4-SiO_2 photocatalyst.

FIGURE 2: Schematic diagram of the photoreactor.

FIGURE 3: Effect of TFS catalyst loading on the degradation of naphthalene. Inset graph: rate constant (k) versus TFS catalyst loading.

The optimum concentration of the TFS photocatalyst was examined by varying the catalyst amount from 0.25 to 1.50 g/L. The reaction rates (k) were estimated by fitting the time-course curves using the first-order kinetics [14, 30], which was presented in the inset of Figure 3. It can be seen from Figure 2 that, as the TFS photocatalyst loading increased, the photocatalytic efficiency of the degradation increased firstly and then decreased. At 1.00 g/L catalyst loading, the first-order rate constant k reached maximum and the rate of degradation reached a saturation value. By further increasing the catalyst loading, it would lead to the aggregation of the catalyst particles, which, in turn, resulted in the decrease of active sites and the naphthalene photodegradation. Consequently, the operating range of catalyst loading for multivariate experimental design was 0.8–1.0 g/L, taking costs into account simultaneously.

3.2. Effect of pH on Degradation of Naphthalene. It is known that the influence of pH to the photodegradation is substantially complex, which can directly affect the surface charged properties of photocatalyst particles and, by extension, influence the adsorption behavior of substrate molecules on the photocatalyst surface. In the present study, therefore, it was chosen as a predominant operational factor for the photooxidative degradation of naphthalene. Metal oxide particles suspended in water behaved similar to diprotic acids.

When TiO_2 surface was hydrated, the principal surface functionality was the amphoteric "Titanol" moiety, $-TiOH$, which took part in the following acid-base equilibrium [31]:

$$-TiOH + H^+ = TiOH^+_2, \quad pK^S_{a1}, \tag{3}$$

$$TiO^- + H^+ = -TiOH, \quad pK^S_{a2}, \tag{4}$$
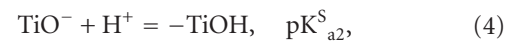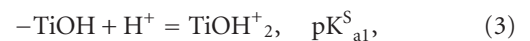
where pK^S_{a1} and pK^S_{a2} represented the negative log of the acidity constants of the first and second acid dissociation, respectively. The pH of zero point of charge, pH_{zpc}, was given as the following equation:

$$pH_{zpc} = 0.5\left(pK^S_{a1} + pK^S_{a2}\right). \tag{5}$$

In the TFS photocatalyst, TiO_2 spreads as a layer over Fe_3O_4-SiO_2 core (Figure 1). Thus as far as surface properties be concerned, TFS was similar to pure TiO_2. For TiO_2 Degussa P-25, the corresponding surface acidity constants are found to be $pK^S_{a1} = 4.5$ and $pK^S_{a2} = 8.0$, and pH_{zpc} has been determined by titration: $pH_{zpc} = 6.3$ [32].

Figure 4 presents the variation of the first-order rate constant and the value of Ct/Co as a function of pH. The catalyst loading was 1.0 g/L. It can be noticed that a higher
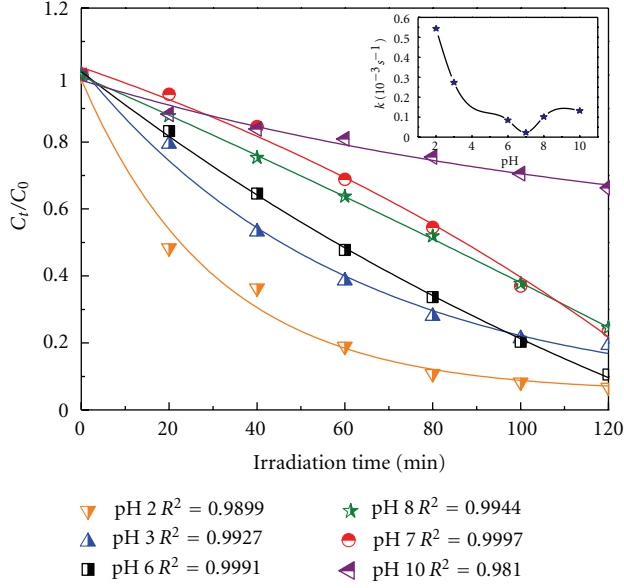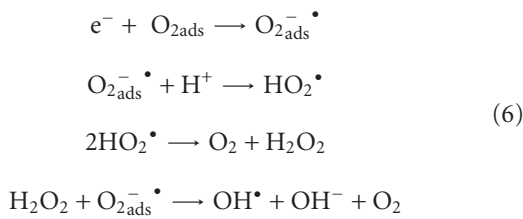
FIGURE 4: Effect of pH on the degradation of naphthalene. Inset graph: rate constant (k) versus pH.

photodegradation effect existed in acid environment, which was assumed to be linked with the surface characteristic of TFS photocatalyst particles. At low pH, hydroxyl radicals were formed on the surface of TFS particles by the reaction of hole (h_{vb}^+) with adsorbed H_2O molecule: $h_{vb}^+ + H_2O \rightarrow OH^\bullet + H^+$, which made electron ($e^-$) assemble to the surface of TFS particles and then reacted with adsorbed O_2 to $O_2^{-\bullet}$, leading to longer lifetime of the electron/hole pair [33]. Moreover, the increased hydrogen ions was beneficial to the production of H_2O_2 and $OH^\bullet$ radicals. The specific reactions were given as follows.

$$
\begin{aligned}
e^- + O_{2ads} &\longrightarrow O_{2ads}^{-\bullet} \\
O_{2ads}^{-\bullet} + H^+ &\longrightarrow HO_2^\bullet \\
2HO_2^\bullet &\longrightarrow O_2 + H_2O_2 \\
H_2O_2 + O_{2ads}^{-\bullet} &\longrightarrow OH^\bullet + OH^- + O_2
\end{aligned}
\tag{6}
$$

At high pH, the TFS particles' surface was negatively charged which increased the work function for electron abjection and also trapped of valence-band holes. It made against the photocatalytic reaction. But the reaction rates in pH 8 and 10 were a little increased than those in neutral in this case, because the solutions at different pH had different ionic strength: HNO_3 was present at acid solution and NaOH was present at alkaline solution, whereas no ionic species were added at neutral pH 7, and additionally the quantities of ionic also affected the ionic strength.

As seen in the inset of Figure 4, the first-order rate constant of the degradation (k) at pH 2 was higher than those at other pH values. As a consequence, the operating range of pH for multivariate experimental design was 1.5–2.5.

TABLE 1: Effect of irradiation time on the degradation of naphthalene.

Irradiation time (min)	20	40	60	80	100	120
Degradation rate (%)	51.6	63.6	81.0	89.2	91.7	93.3

3.3. Effect of Irradiated Time on Degradation of Naphthalene. Table 1 shows the variation of the degradation rate in the condition of optimal catalyst loading (1.00 g/L) and pH (2) as a function of irradiation time.

As displayed in Table 1, the increase of degradation rate went flatter after 80 min. The degradation rate enhanced 2.5% in the time range of 80~100 min, while the degradation rate enhanced only 1.51% in the time range of 100~120 min which was much lower than the previous three ranges. The irradiation time counted little to the degradation rate of naphthalene after 80 min. Consequently, the operating range of irradiation time for multivariate experimental design was 80–100 min, taking costs into account simultaneously.

3.4. Optimization of Operational Parameters for Enhancing the Naphthalene Degradation. Experimental design and results are shown in Table 2. By applying multiple regression analysis on the experimental data, a second-order polynomial equation was obtained to describe the correlation between the independent variable and the naphthalene degradation rate:

$$
\begin{aligned}
y = {} & -1262.32 + 15.63x_1 + 54.20x_2 \\
& + 1130.84x_3 - 0.11x_1x_2 - 2.56x_1x_3 \\
& + 19.5x_2x_3 - 0.067x_1^2 - 14.81x_2^2 - 480.26x_3^2,
\end{aligned}
\tag{7}
$$

where y is the predicted naphthalene degradation rate (%); x_1, x_2, and x_3 are irradiation time (min), pH value, and catalyst loading (g/L), respectively.

The analysis of variance (ANOVA) was conducted to test the significance of the fit of the second-order polynomial equation for the degradation rate as shown in Table 3.

The F value, represented the likelihood of two different groups being statistically different, was 551.40 which implied that the model was significant because values of "Prob > F" less than 0.05 were considered to be significant. There was only less 0.01% chance that a model F value this large could occur; the regression mathematical model was a good fit to experimental data. In addition, the model did not show lack of fit. The Pred R-squared was 0.9827 which was in reasonable agreement with the Adj R-squared (0.9964). The disparity of R-squared (0.9982) and Adj R-squared was probably originated in the insignificance of x_1x_2 term. The Adeq Precision was 64.080 which indicated an adequate signal, measuring the signal to noise ratio. Myers pointed that model adequacies should be checked by R^2, Adj-R^2, Pre-R^2, Adeq. Precision, and CV (lack of fit > 0.1; $R^2 > 0.95$; (Adj-R^2–Pre-R^2) < 0.2; CV < 10; Pre-$R^2 > 0.7$; Adeq. Precision > 4) [34]. After calculated, R^2, Adj-R^2, Pre-R^2, Adeq. Precision and coefficient of variation (CV, 1.00) all satisfied the request of model adequacy; therefore, (7) properly described the degradation rate of naphthalene in this study. From (7),

TABLE 2: The central composite experimental design with three independent variables and results.

Run	Irradiation time (min)	Code x_1	pH	Code x_2	Catalyst loading (g/L)	Code x_3	Degradation rate y (%)
			Factors (coded value)				
1	80	+1	1.5	+1	0.8	+1	54.5
2	100	−1	1.5	+1	0.8	+1	81.3
3	80	+1	2.5	−1	0.8	+1	55.3
4	100	−1	2.5	−1	0.8	+1	82.4
5	80	+1	1.5	+1	1.0	−1	71.3
6	100	−1	1.5	+1	1.0	−1	90.3
7	80	+1	2.5	−1	1.0	−1	78.5
8	100	−1	2.5	−1	1.0	−1	92.8
9	90	0	2.0	0	0.9	0	91.0
10	90	0	2.0	0	0.9	0	90.5
11	90	0	2.0	0	0.9	0	91.1
12	90	0	2.0	0	0.9	0	90.2
13	90	0	2.0	0	0.9	0	91.1
14	90	0	2.0	0	0.9	0	91.6
15	73.18	−a	2.0	0	0.9	0	52.6
16	106.82	a	2.0	0	0.9	0	91.4
17	90	0	1.16	−a	0.9	0	78.7
18	90	0	2.84	A	0.9	0	82.0
19	90	0	2.0	0	0.7318	−α	64.3
20	90	0	2.0	0	1.0682	α	90.2

TABLE 3: Analysis of variance (ANOVA) for the model regression representing degradation rate.

Source	Sum of squares	df	Mean square	F value	P value (Prob $> F$)
Model	3557.63	9	395.29	551.40	<0.0001
x_1	1707.76	1	1707.76	2382.18	<0.0001
x_2	21.57	1	21.57	30.09	0.0004
x_3	774.28	1	774.28	1080.06	<0.0001
$x_1 x_2$	2.49	1	2.49	3.47	0.0955
$x_1 x_3$	52.33	1	52.33	72.99	<0.0001
$x_2 x_3$	7.64	1	7.64	10.66	0.0098
x_1^2	638.82	1	638.82	891.10	<0.0001
x_2^2	197.46	1	197.46	275.44	<0.0001
x_3^2	332.13	1	332.13	463.30	<0.0001
Residual	6.45	9	0.72		
Lack of fit	5.84	5	1.17	7.64	0.036
Cor total	3565.48	19			

the optimal values of x_1, x_2, and x_3 in the actual units were found to be 97.1 min irradiation time, 2.1 pH, and 0.962 g/L catalyst loading, respectively. The maximum predicted value of degradation rate obtained was 97.39%.

Figures 5–7 show the response surface plots and corresponding contour plots based on (7) with one variable being kept constant at its optimum level and the other two variables varied within the experimental range. As can be seen from Figures 4–6, the response surface of degradation rate showed a clear peak, indicating that the optimum conditions were inside the design boundary well. Degradation rate increased with irradiation time, pH, and catalyst loading to optimum conditions, respectively, and then decreased with a further increase. This result indicates that irradiation time, pH, and
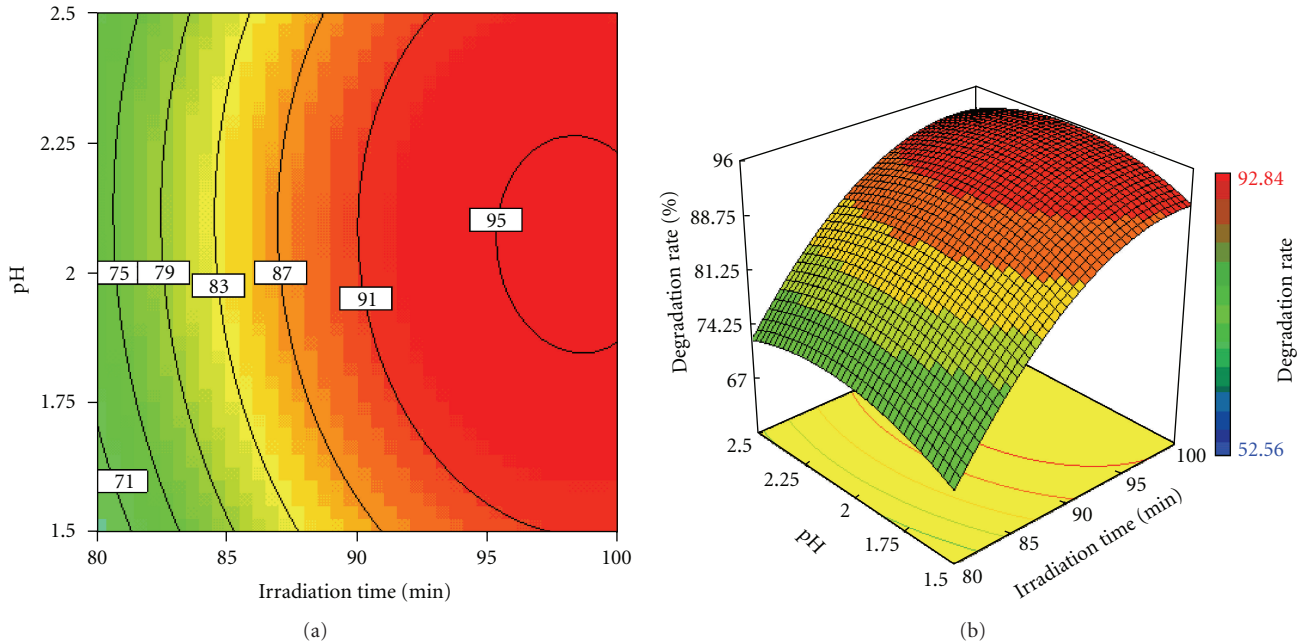
(a)

(b)

FIGURE 5: The response surface plot and the corresponding contour plot showing the effects of irradiation time and pH on naphthalene degradation rate.
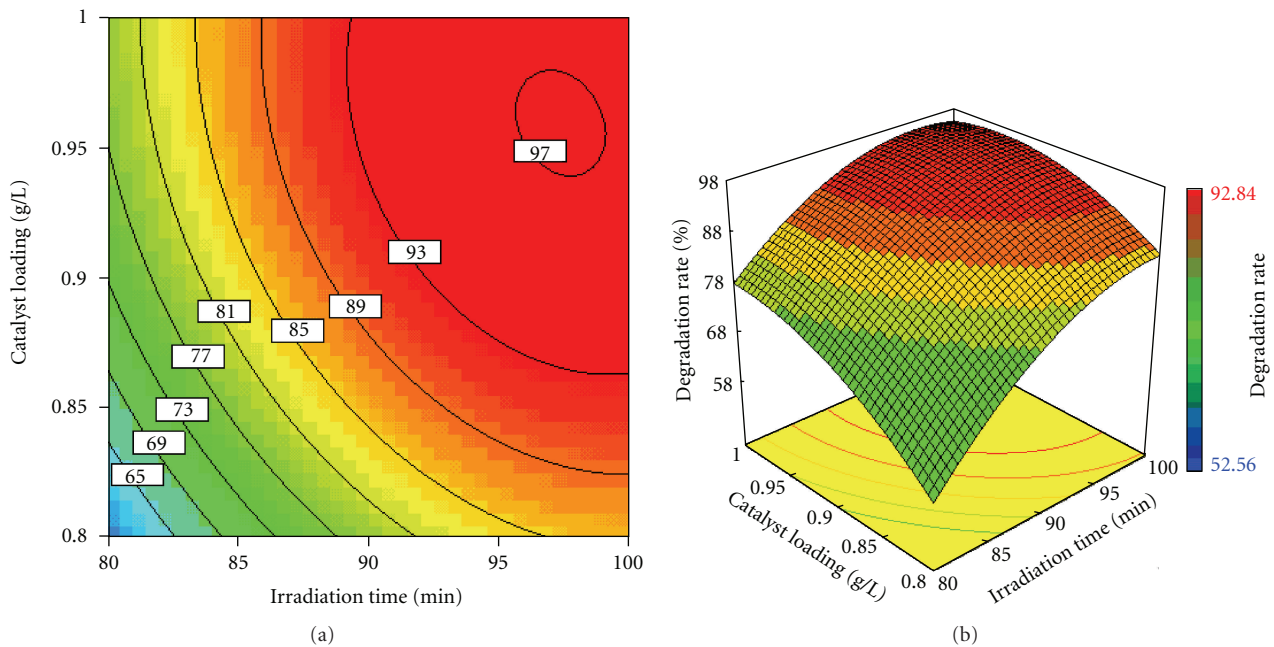

(a)

(b)

FIGURE 6: The response surface plot and the corresponding contour plot showing the effects of irradiation time and catalyst loading on naphthalene degradation rate.

catalyst loading all had individual significant influences on degradation rate. In addition, the angle of inclination of the principal axis was evidently towards either irradiation time or catalyst loading in Table 1 and Figure 3, respectively, and this indicated that the positive effect of increased irradiation time or catalyst loading levels on degradation rate was more pronounced than pH increased.

3.5. Validation of the Model. In order to confirm the validity of the statistical experimental strategy, the repeated experiments under optimal conditions were carried out (Table 4). As a consequence, the maximum standard error between the observed value and the predicted value was less than 4% which indicated that the quadratic model can predict experimental results well. Furthermore, the standard
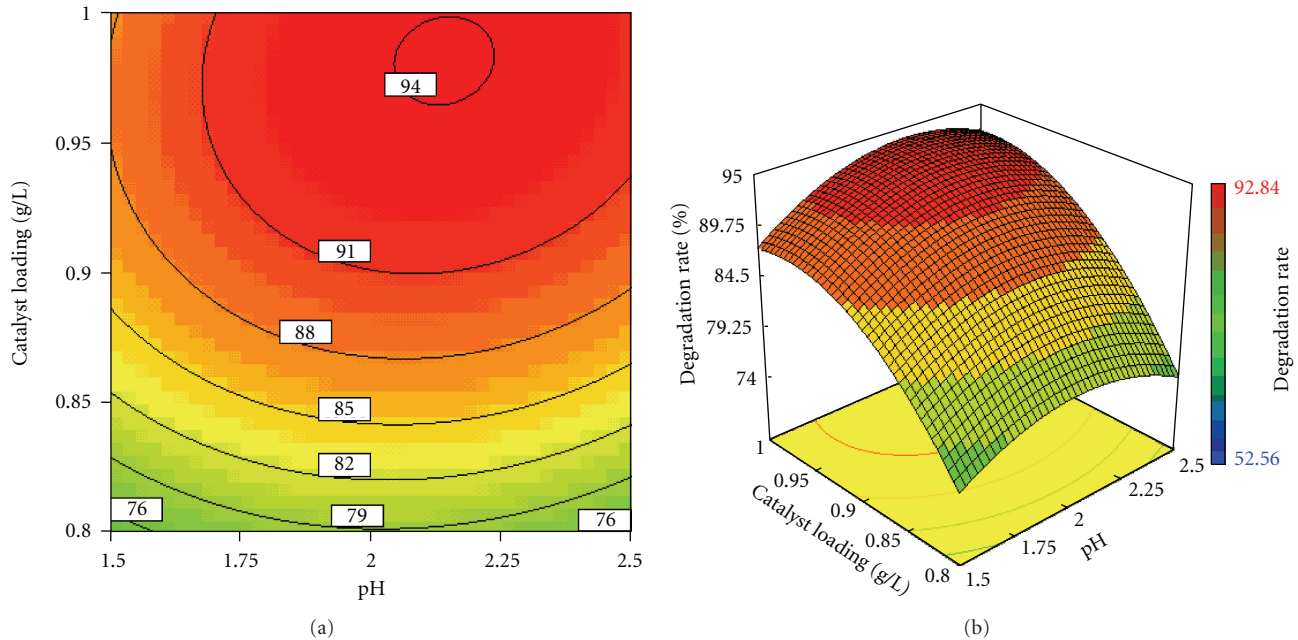
(a)

(b)

FIGURE 7: The response surface plot and the corresponding contour plot showing the effects of pH and catalyst loading on naphthalene degradation rate.

TABLE 4: Confirm analyses for the model on naphthalene removal.

Codes	Factors (coded value)			Degradation rate y (%)		Standard error (%)
	Irradiation time (min)	pH value	Catalyst loading (g/L)	Actual value	Predicted value	
1	90	1.5	0.80	71.9	74.6	3.63
2	100	2	0.90	92.8	95.5	2.79
3	120	2.5	0.80	55.7	54.8	2.26
4	97.1	2.1	0.962	95.9	97.4	1.55
5	97.1	2.1	0.962	96.3	97.4	1.07
6	97.1	2.1	0.962	97.0	97.4	0.37

error was only 2.26% in code 3 when the irradiation time (120 min) was beyond the operating range for multivariate experimental design, from which we can see that the model had extrapolation ability. As been shown, the degradation rate of naphthalene was 95.88%, 96.34%, and 97.03% in the optimal experimental condition, respectively. The observed values enhanced about 4% than nonoptimal experimental values at the same temperature.

4. Conclusions

The present study focused on the optimization of operational parameters for enhancing naphthalene degradation by TiO_2/Fe_3O_4-SiO_2 photocatalyst using the statistical methodology. Based on the central composite design, the maximum predicted value of degradation rate was obtained when the operational parameters were 97.1 min irradiation time, 2.1 pH, and 0.962 g/L catalyst loading, respectively. The high correlation between the predicted and observed values indicated the validity of the model. This result suggested that statistical design methodology offers an efficient and feasible approach for optimization the operational parameters of naphthalene degradation by TiO_2/Fe_3O_4-SiO_2 photocatalyst.
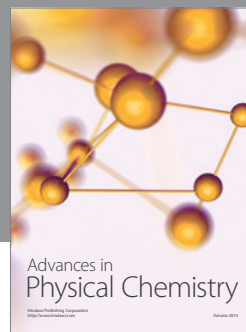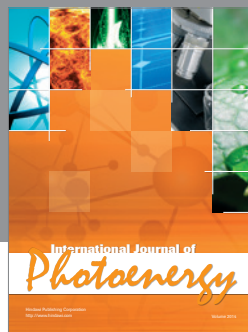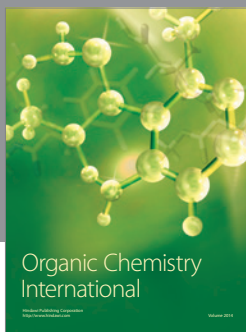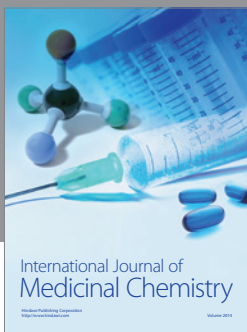
References

[1] S. C. Wilson and K. C. Jones, "Bioremediation of soil contaminated with polynuclear aromatic hydrocarbons (PAHs): a review," *Environmental Pollution*, vol. 81, no. 3, pp. 229–249, 1993.

[2] B. Guieysse, M. D. Cirne, and B. Mattiasson, "Microbial degradation of phenanthrene and pyrene in a two liquid phase-partitioning bioreactor," *Applied Microbiology and Biotechnology*, vol. 56, pp. 796–802, 2001.

[3] A. Lair, C. Ferronato, J. M. Chovelon, and J. M. Herrmann, "Naphthalene degradation in water by heterogeneous photocatalysis: an investigation of the influence of inorganic anions," *Journal of Photochemistry and Photobiology A*, vol. 193, no. 2-3, pp. 193–203, 2008.

[4] K. Maillacheruvu and S. Safaai, "Naphthalene removal from aqueous systems by Sagittarius sp," *Journal of Environmental Science and Health Part A*, vol. 37, no. 5, pp. 845–861, 2002.

[5] H. Pathak, D. Kantharia, A. Malpani, and D. Madamwar, "Naphthalene degradation by Pseudomonas sp. HOB1: in vitro studies and assessment of naphthalene degradation efficiency in simulated microcosms," *Journal of Hazardous Materials*, vol. 166, no. 2-3, pp. 1466–1473, 2009.

[6] Y. Jia, H. Yin, J. S. Ye et al., "Characteristics and pathway of naphthalene degradation by pseudomonas sp. N7," *Journal of Environmental Science*, vol. 29, no. 3, pp. 756–762, 2008.

[7] F. Musat, A. Galushko, J. Jacob et al., "Anaerobic degradation of naphthalene and 2-methylnaphthalene by strains of marine sulfate-reducing bacteria," *Environmental Microbiology*, vol. 11, no. 1, pp. 209–219, 2009.

[8] J. Dou, X. Liu, and A. Ding, "Anaerobic degradation of naphthalene by the mixed bacteria under nitrate reducing conditions," *Journal of Hazardous Materials*, vol. 165, no. 1–3, pp. 325–331, 2009.

[9] M. Safinowski and R. U. Meckenstock, "Methylation is the initial reaction in anaerobic naphthalene degradation by a sulfate-reducing enrichment culture," *Environmental Microbiology*, vol. 8, no. 2, pp. 347–352, 2006.

[10] W. J. Cooper, M. G. Nickelsen, R. V. Green, and S. P. Mezyk, "The removal of naphthalene from aqueous solutions using high-energy electron beam irradiation," *Radiation Physics and Chemistry*, vol. 65, no. 4-5, pp. 571–577, 2002.

[11] R. K. Goel, J. R. V. Flora, and J. Ferry, "Mechanisms for naphthalene removal during electrolytic aeration," *Water Research*, vol. 37, no. 4, pp. 891–901, 2003.

[12] E. Pramauro, A. B. Prevot, M. Vincenti, and R. Gamberini, "Photocatalytic degradation of naphthalene in aqueous TiO_2 dispersions: effect of non ionic surfactants," *Chemosphere*, vol. 36, no. 7, pp. 1523–1542, 1998.

[13] S. Dass, M. Muneer, and K. R. Gopidas, "Photocatalytic degradation of wastewater pollutants. Titanium-dioxide-mediated oxidation of polynuclear aromatic hydrocarbons," *Journal of Photochemistry and Photobiology A*, vol. 77, no. 1, pp. 83–88, 1994.

[14] L. Hykrdová, J. Jirkovský, G. Mailhot, and M. Bolte, "Fe(III) photoinduced and Q-TiO_2 photocatalysed degradation of naphthalene: comparison of kinetics and proposal of mechanism," *Journal of Photochemistry and Photobiology A*, vol. 151, no. 1–3, pp. 181–193, 2002.

[15] S. V. Mohan, T. Kisa, T. Ohkuma, R. A. Kanaly, and Y. Shimizu, "Bioremediation technologies for treatment of PAH-contaminated soil and strategies to enhance process efficiency," *Reviews in Environmental Science and Biotechnology*, vol. 5, no. 4, pp. 347–374, 2006.

[16] M. Lindner, J. Theurich, and D. W. Bahnemann, "Photocatalytic degradation of organic compounds: accelerating the process efficiency," *Water Science and Technology*, vol. 35, no. 4, pp. 79–86, 1997.

[17] T. Ohno, K. Tokieda, S. Higashida, and M. Matsumura, "Synergism between rutile and anatase TiO_2 particles in photocatalytic oxidation of naphthalene," *Applied Catalysis A*, vol. 244, no. 2, pp. 383–391, 2003.

[18] B. Pal and M. Sharon, "Photodegradation of polyaromatic hydrocarbons over thin film of TiO_2 nanoparticles; a study of intermediate photoproducts," *Journal of Molecular Catalysis A*, vol. 160, no. 2, pp. 453–460, 2000.

[19] N. Barrios, P. Sivov, D. D'Andrea, and O. Núñez, "Conditions for selective photocatalytic degradation of naphthalene in triton X-100 water solutions," *International Journal of Chemical Kinetics*, vol. 37, no. 7, pp. 414–419, 2005.

[20] M. J. García-Martínez, L. Canoira, G. Blázquez, I. Da Riva, R. Alcántara, and J. F. Llamas, "Continuous photodegradation of naphthalene in water catalyzed by TiO_2 supported on glass Raschig rings," *Chemical Engineering Journal*, vol. 110, no. 1–3, pp. 123–128, 2005.

[21] J.-P. Wang, Y.-Z. Chen, Y. Wang, S.-J. Yuan, and H.-Q. Yu, "Optimization of the coagulation-flocculation process for pulp mill wastewater treatment using a combination of uniform design and response surface methodology," *Water Research*, vol. 45, no. 17, pp. 5633–5640, 2011.

[22] I. H. Cho and K. D. Zoh, "Photocatalytic degradation of azo dye (Reactive Red 120) in TiO_2/UV system: optimization and modeling using a response surface methodology (RSM) based on the central composite design," *Dyes and Pigments*, vol. 75, no. 3, pp. 533–543, 2007.

[23] A. F. Caliman, C. Cojocaru, A. Antoniadis, and I. Poulios, "Optimized photocatalytic degradation of Alcian Blue 8 GX in the presence of TiO_2 suspensions," *Journal of Hazardous Materials*, vol. 144, no. 1-2, pp. 265–273, 2007.

[24] J. F. Fu, Y. Q. Zhao, X. D. Xue, W. C. Li, and A. O. Babatunde, "Multivariate-parameter optimization of acid blue-7 wastewater treatment by Ti/TiO_2 photoelectrocatalysis via the Box-Behnken design," *Desalination*, vol. 243, no. 1–3, pp. 42–51, 2009.

[25] A. R. Khataee, M. Zarei, and S. K. Asl, "Photocatalytic treatment of a dye solution using immobilized TiO_2 nanoparticles combined with photoelectro-Fenton process: optimization of operational parameters," *Journal of Electroanalytical Chemistry*, vol. 648, no. 2, pp. 143–150, 2010.

[26] M. Fathinia, A. R. Khataee, M. Zarei, and S. Aber, "Comparative photocatalytic degradation of two dyes on immobilized TiO_2 nanoparticles: effect of dye molecular structure and response surface approach," *Journal of Molecular Catalysis A*, vol. 333, no. 1-2, pp. 73–84, 2010.

[27] L. Y. Wang, H. X. Wang, A. J. Wang, and M. Liu, "Surface modification of a magnetic SiO_2 support and immobilization of a nano-TiO_2 photocatalyst on it," *Chinese Journal of Catalysis*, vol. 30, no. 9, pp. 939–944, 2009.

[28] S. L. Akhnazarova and V. V. Kafarov, *Experiment Optimization in Chemistry and Chemical Engineering*, Mir Publishers, Moscow, Russia, 1982.

[29] H. G. Neddermeijer, G. J. van Oortmarssen, N. Piersma, and R. Dekker, "Framework for Response Surface Methodology for simulation optimization," in *Proceedings of the 32nd Winter Simulation Conference Proceedings*, pp. 129–136, Orlando, Fla, USA, December 2000.

[30] E. Pramauro, A. B. Prevot, M. Vincenti, and R. Gamberini, "Photocatalytic degradation of naphthalene in aqueous TiO_2 dispersions: effect of non ionic surfactants," *Chemosphere*, vol. 36, no. 7, pp. 1523–1542, 1998.

[31] M. R. Hoffmann, S. T. Martin, W. Choi, and D. W. Bahnemann, "Environmental applications of semiconductor photocatalysis," *Chemical Reviews*, vol. 95, no. 1, pp. 69–96, 1995.

[32] N. Jaffrezic-Renault, P. Pichat, A. Foissy, and R. Mercier, "Study of the effect of deposited platinum particles on the surface charge of titania aqueous suspensions by potentiometry, electrophoresis, and labeled-ion adsorption," *Journal of Physical Chemistry*, vol. 90, pp. 2733–2738, 1986.

[33] D. Duonghong, J. Ramsden, and M. Grätzel, "Dynamics of interfacial electron-transfer processes in colloidal semiconductor systems," *Journal of the American Chemical Society*, vol. 104, no. 11, pp. 2977–2985, 1982.

[34] R. H. Myers, D. C. Montgomery, and C. M. Anderson-Cook, *Response Surface Methodology: Process and Product Optimization Using Designed Experiments*, John Wiley & Sons, Hoboken, NJ, USA, 2002.